Scientific Research Publishing

Open Journal of Inorganic Chemistry, 2017, 7, 102-115
http://www.scirp.org/journal/ojic
ISSN Online: 2161-7414
ISSN Print: 2161-7406

# Synthesis, Rietveld Refinement and DFT Studies of Bis(4,5-dihydro-1*H*-benzo[g]indazole)silver(I) Hexafluorophosphate Complex Salt

**Tanyi Rogers Fomuta[1], Jean Ngoune[1*], Golngar Djimassingar[1,2], Tayo Alain Djampouo[1], Junior Ma Ntep Tobie Matemb[1], Jean Jacques Anguile[3], Justin Nenwa[4*]**

[1]Department of Chemistry, University of Dschang, Dschang, Cameroon
[2]Department of Chemistry, Mongo Polytechnique University Institute (IUPM), Mongo, Tchad
[3]Department of Chemistry, University of Sciences & Techniques of Masuku, Franceville, Gabon
[4]Department of Inorganic Chemistry, University of Yaounde 1, Yaounde, Cameroon
Email: *jean.ngoune@univ-dschang.org, *jnenwa@yahoo.fr

**How to cite this paper:** Fomuta, T.R., Ngoune, J., Djimassingar, G., Djampouo, T.A., Matemb, J.M.N.T., Anguile, J.J. and Nenwa, J. (2017) Synthesis, Rietveld Refinement and DFT Studies of Bis(4,5-dihydro-1*H*-benzo[g]indazole)silver(I) Hexafluorophosphate Complex Salt. *Open Journal of Inorganic Chemistry*, **7**, 102-115.
https://doi.org/10.4236/ojic.2017.74007

**Received:** September 8, 2017
**Accepted:** October 27, 2017
**Published:** October 30, 2017



## Abstract

The new salt bis(4,5-dihydro-1*H*-benzo[g]indazole)silver(I) hexafluorophosphate, $[Ag(N_2H_{10}C_{11})_2]PF_6$, has been synthesized in methanol at ambient temperature and characterized by elemental and thermal analyses, FTIR and $^1$HNMR spectroscopies, Rietveld refinement from powder diffraction data and DFT studies. The salt crystallizes in the triclinic space group *P*-1 with the parameters: $a$ = 7.776 Å, $b$ = 8.676 Å, $c$ = 9.226 Å, $\alpha$ = 69.27˚ $\beta$ = 89.86˚, $\gamma$ = 74.50˚, $V$ = 558.02 Å$^3$, $Z$ = 1. In the structure, the silver center is coordinated to two nitrogen atoms from two 4,5-dihydro-1*H*-benzo[g]indazole ligands, forming a centrosymmetric complex cation, $[Ag(N_2H_{10}C_{11})_2]^+$, with a linear coordination geometry around the silver center. The hexafluorophosphate ion, $PF_6^-$, acts as counter anion. The crystal packing is governed by N-H···F and C-H···F hydrogen bonds that interconnect the ionic constituents and Ag···F and Ag···π interactions help for the stabilization of the packing. The optimized structure was obtained at B3LYP/LanL2DZ level in the gas phase. The stability and reactivity of the structure were studied using respectively HOMO-LUMO gap and electronic global quantities (ionization potential (I) and electron affinity (A)) as descriptors.

## Keywords

Silver Complex Salt, 4,5-dihydro-1*H*-benzo[g]indazole, $^1$HNMR, Powder Diffraction, Rietveld Refinement, DFT

## 1. Introduction

Pyrazole is a five-membered heterocycle, made up of three carbon atoms and two nitrogen atoms in adjacent positions. Numerous compounds containing this organic molecule are known to exhibit anti-hyperglycemic, analgesic, anti-inflammatory, antipyretic, antibacterial, antimicrobial, antihypertensive and antidepressant activities [1] [2] [3]. The coordination chemistry of pyrazole derivatives continues receiving considerable attention, due to the ability of these molecules to act as remarkably flexible ligand systems in complexation with a wide range of metal ions [4] [5] [6]. They easily coordinate metal centers through their N2 atoms and also form interesting hydrogen interactions. Metal complexes of pyrazole derivatives often yield unusual electronic and steric properties that can be fine-tuned nearly at will [7] [8]. They find applications in antipyretics and antirheumatics, in herbicides, in fungicides, and also as metal ion extractants [9] [10]. Furthermore, pyrazole complexes exhibit luminescence, anticancer and anti-HIV activities [11] [12] [13]. In living organisms, metal ions are usually bonded to the imidazole unit of hystidine, which is a part of proteins. In view of the similarity of pyrazole and imidazole, pyrazole metal complexes are suitable agents to mimic enzymatic reactions [14].

The pyrazole derivative, 4,5-dihydro-1*H*-benzo[g]indazole, is a bulky ligand synthesized and characterized by Trofimenko and co-workers [15]. Very recently, investigation of the coordination reactivity of this versatile pyrazole ligand towards silver(I) nitrate in methanol led to formation of a pseudo linear bis(4,5-dihydro-1*H*-benzo[g]indazole)silver(I) nitrate ($[Ag(N_2H_{10}C_{11})_2]NO_3$) adduct [16]. In continuation of this research program which aims to deepen the coordination ability of pyrazole derivatives, we report herein the synthesis, characterization and DFT studies of bis(4,5-dihydro-1*H*-benzo[g]indazole)silver(I) hexafluorophosphate complex salt, $[Ag(N_2H_{10}C_{11})_2]PF_6$, the crystallographic structure of which was assessed through Rietveld refinement from powder diffraction data.

## 2. Experimental

### 2.1. Materials and Experimental Procedures

All chemicals were purchased from Aldrich and used as received. The ligand, 4,5-dihydro-1*H*-benzo[g]indazole was prepared following Trofimenko's reported procedure [15]. The synthesis of the complex was carried out in air. Melting point was measured and uncorrected using an SMP3 Stuart Scientific instrument operating at a ramp rate of 1.5˚C/min. Elemental analysis (C, H, N) was performed with a Fisson Instrument 1108 CHNS-O elemental analyzer, while the thermogravimetric analysis was obtained using a Perkin-Elmer STA 6000 thermo-balance. The IR spectrum was recorded from 4000 - 650 $cm^{-1}$ with a Perkin-Elmer System 100 FT-IR spectrophometer. $^1$HNMR spectrum was recorded on a Mercury Plus Variant 400 spectrophotometer operating at room temperature. Proton chemical shift (δ) values are reported in parts per million

(ppm) from $SiMe_4$ (calibrating by internal deuterium solvent lock). Peak multiplicities are abbreviated as: singlet, s; doublet, d; triplet, t; quartet, q and multiplet, m. The X-ray powder diffraction (XRPD) data were measured at room temperature, in air. Fortunately, the compound gave traces of decent quality, allowing a fruitful structural determination. Some amount of the sample was gently ground in an agate mortar, and then deposited in the hollow of a 0.2 mm deep aluminum sample holder, equipped with a quartz monocrystal zero background plate (supplied by the Gem Dugout, State College, PA). Diffraction data were collected in the 5 - 105˚ 2θ range, sampling at 0.02˚, on a θ:θ vertical scan Bruker AXS D8 Advance diffractometer, equipped with a linear Lynxeye position sensitive detector, set at 300 mm from the sample. Ni-filtered Cu $K\alpha_{1,2}$ radiation, λ = 1.5418 Å. Standard peak search methods, followed by indexing by TOPAS-R [17], allowed the determination of approximate cell parameters; systematic absences allowed the detection of the probable space groups, later confirmed by successful structure solutions and refinements. Structure solution was initiated by employing a semi-rigid molecular fragment for 4,5-dihydro-1*H*-benzo[g]indazole, flexible about two torsion angles, and free silver, phosphorus and fluoride atoms. Hydrogen atoms have been positioned in idealized locations as they have been included in the definition of the rigid bodies. Simulated annealing (occasionally helped by soft restraints) allowed the location and orientation of the used fragments, later refined by the Rietveld method. The fundamental parameter approach in describing the peak shapes was employed, the background contribution was modeled by a polynomial fit, and preferred orientation effects (010 pole) were described by the March-Dollase formulation [18] [19]. A single isotropic thermal parameter was adopted for the Ag atom, while lighter atoms were assigned $B = B_{Ag} + 2.0$ Å$^2$. Structure solution and refinements were performed by TOPAS-R.

The optimization of the experimental structure at the B3LYP/LanL2DZ level was performed using the Gaussian 09 program [20] and was followed by the vibrational frequency and the HOMO-LUMO gap calculations. In the whole, HOMO-LUMO gap is used to measure the stability indicators. The electron affinity (A) and ionization potential (I) respectively defined by Equation (1)-(2) are used as global reactivity descriptors of the synthesized complexes.

$$I = -E_{\mathrm{HOMO}} \tag{1}$$

$$A = -E_{LUMO} \tag{2}$$

where, $E_{\mathrm{HOMO}}$ and $E_{\mathrm{LUMO}}$ are respectively energy values of HOMO (highest occupied molecular orbital) and LUMO (lowest unoccupied molecular orbital). Additional global quantities can be built from these previous parameters such as chemical hardness $(\eta)$ [21], chemically soft ($S$), chemical potential ($\mu$) and global electrophilicity index ($\omega$) respectively defined as followed.

$$\eta = \frac{I - A}{2} \tag{3}$$

$$S = \frac{1}{2\eta} \tag{4}$$

$$\mu = -\frac{(I + A)}{2} \tag{5}$$

$$\omega = \frac{\mu^2}{2\eta} \tag{6}$$

It is important to mention that chemical hardness $(\eta)$ is associated with the stability of the compound because it measures the ability of the compound to resist changes in its electron distribution or charge transfer. High values of chemical hardness indicate more stability and low reactivity of the compound. On the other hand, molecules with small values of $\eta$ are said to be chemically soft and are highly polarizable and more chemically reactive. Chemical potential ($\mu$) is a quantity that measures the escaping tendency of electrons from this compound in its ground state. High values of chemical potential signify that the molecule is less stable and more reactive [22]. The global electrophilicity index ($\omega$) measures the stabilization in energy of a system, when it acquires an additional electronic charge from the environment [23].

### 2.2. Synthesis

The compound $[Ag(N_2H_{10}C_{11})_2]PF_6$ was synthesized through the reaction of 4,5-dihydro-1*H*-benzo[g]indazole with silver(I) hexafluorophosphate in methanol, at ambient temperature according to Equation (7).

$$AgPF_6 + 2C_{11}H_{10}N_2 \xrightarrow[AT]{MeOH} \left[Ag\left(N_2H_{10}C_{11}\right)_2\right]PF_6 \tag{7}$$

In a 50 mL round bottom flask containing 25 mL of methanol was introduced 0.05 g (0.29 mmol) of silver hexafluorophosphate ($AgPF_6$) which was dissolved upon magnetic agitation at ambient temperature. To this stirred solution, 0.10 g (0.58 mmol) of 4,5-dihydro-1*H*-benzo[g]indazole ($C_{11}H_{10}N_2$) was added in successive small portions. The mixture was stirred overnight and then filtered. The resulting colorless solution was allowed to evaporate in a hood at room temperature. A colorless microcrystalline material unsuitable for single crystal X-ray diffraction was harvested within few days in 82.5% yield.

## 3. Results and Discussion

### 3.1. Physical Properties and Elemental Analysis

The synthesized complex salt is insoluble in $H_2O$ and slightly soluble in $CH_2Cl_2$ or $CHCl_3$. This colorless solid melts at 247 - 249˚C. The experimental values obtained from elemental analysis are in agreement with theoretical values as illustrated on **Table 1** and confirms that the synthesized compound is actually bis(4,5-dihydro-1*H*-benzo[g]indazole)silver(I) hexafluorophosphate, $[Ag(N_2H_{10}C_{11})_2]PF_6$.

**Table 1.** Percentage of analyzed elements (C, H, N) in $[Ag(N_2H_{10}C_{11})_2]PF_6$.

| Percentage of C, H, N in $[Ag(N_2H_{10}C_{11})_2]PF_6$ | | | |
|---|---|---|---|
| | % C | % H | % N |
| Theoretical Values | 44.54 | 3.40 | 9.44 |
| Experimental Values | 44.81 | 3.17 | 9.70 |

### 3.2. IR spectrum of $[Ag(N_2H_{10}C_{11})_2]PF_6$

The FTIR spectrum of $[Ag(N_2H_{10}C_{11})_2]PF_6$ shows a characteristic sharp band at 3410 $cm^{-1}$ attributed to the vibration of the N-H group of the pyrazole ring [24] [25]. This band is shifted to higher frequencies of approximately 251 $cm^{-1}$, with respect to that of 4,5-dihydro-1*H*-benzo[g]indazole ligand, occurring between 3159 - 3062 $cm^{-1}$. This indicates that coordination of $AgPF_6$ with the ligand leads to an increase in the IR activity of the N-H group. The variable medium band between 2953 $cm^{-1}$ and 2832 $cm^{-1}$ is attributable to the stretching vibration of C–H of both saturated and unsaturated carbon atoms of the ligand. This absorption band is narrower and less intense compared to that of the free ligand, suggesting that the formation of the $[Ag(N_2H_{10}C_{11})_2]PF_6$ complex is accompanied by a decrease in the IR absorption activity of the C-H group. The variable weak bands between 1618 $cm^{-1}$ and 1543 $cm^{-1}$ are due to C=N and C=C vibrations. The broad (br) intense absorption band at 869 - 767 $cm^{-1}$ indicates the presence of the counter $PF_6^-$ ion. In fact, in the complex $[CuL(NCMe)]PF_6$ (where L= bis(3,5-dimethylpyrazol-1-yl)methane), the hexafluorophosphate anion showed an intense absorption band at 840 $cm^{-1}$ [26].

### 3.3. $^1$H Nuclear Magnetic Resonance Spectrum ($^1$HNMR)

The $^1$HNMR spectrum indicates five families of protons. The N-H hydrogen of the pyrazole ring shows a singlet at $\delta$ = 7.9 ppm (2H, s) while the N=CH-hydrogen presents a singlet at $\delta$ = 7.5 ppm (2H, s). Furthermore, the multiplet at 7.2 ppm (8H, m) is characteristic of aromatic protons and two triplets obtained at $\delta$ = 2.9 ppm (4H, t) and $\delta$ = 2.7 ppm (4H, t) are attributable to two methylene ($CH_2$-$CH_2$) groups of the cyclohexane ring.

### 3.4. Thermogravimetric Analysis

The TG profile of the compound $[Ag(N_2H_{10}C_{11})_2]PF_6$ (**Figure 1**) evidences two distinct weight losses in the temperature range 50 - 600˚C, the two processes being endothermic. The compound $[Ag(N_2H_{10}C_{11})_2]PF_6$ is thermally stable up to 247˚C, followed by a drastic weight loss (45%) between 247 - 300˚C, and a gradual 10% weight loss between 300 - 600˚C. Although these weight losses cannot be attributed to the departure of particular fragments of the material, the loss observed from 247˚C is accompanied by melting and decomposition of $[Ag(N_2H_{10}C_{11})_2]PF_6$.

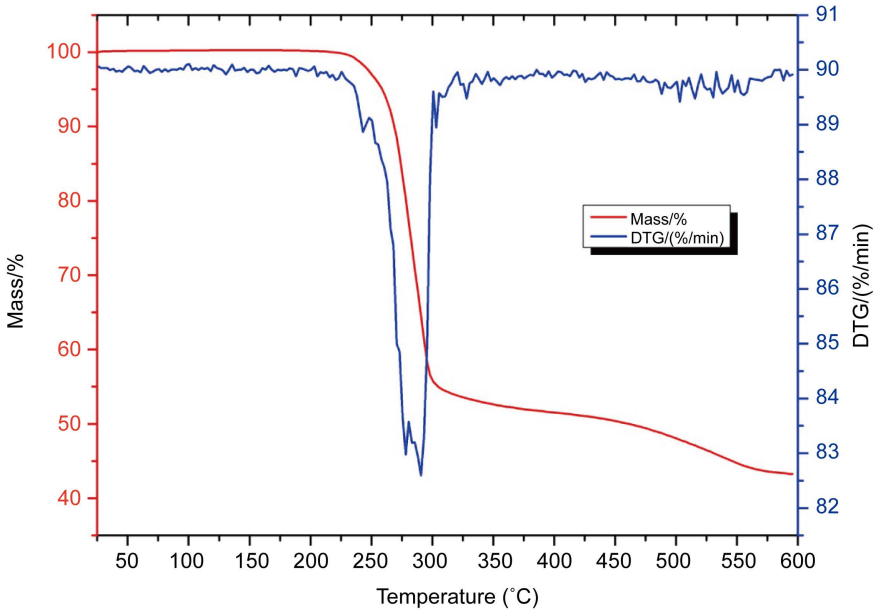


**Figure 1.** TG curve (red) and DTG curve (blue) of $[Ag(N_2H_{10}C_{11})_2]PF_6$.

### 3.5. Crystal Structure of $[Ag(N_2H_{10}C_{11})_2]PF_6$

Single crystal X-ray diffraction technique could not be used to investigate the crystallographic structure of the synthesized compound, due to the poor quality of crystals obtained. Thus, Rietveld refinement from powder diffraction data revealed that the title compound has the formula $[Ag(N_2H_{10}C_{11})_2]PF_6$. The final refinement plot is shown in **Figure 2**, with difference plots and peak markers at the bottom. A summary of crystallographic data is listed in **Table 2**. The MERCURY and the ORTEP views of the title compound are illustrated in **Figure 3**. A projection of the unit cell is presented in **Figure 4** highlighting one $PF_6^-$ anion sandwiching two centrosymmetric $[Ag(N_2H_{10}C_{11})_2]^+$ cations. Selected bond lengths and angles are listed in **Table 3**. Two 4,5-dihydro-1*H*-benzo[g]indazole ligand molecules coordinate to the central silver(I) ion through their pyridine-type N1 atoms, forming a centrosymmetric $[Ag(N_2H_{10}C_{11})_2]^+$ ion with a linear N-Ag-N coordination geometry around the silver(I). The hexafluorophosphate ion, $PF_6^-$, acts as counter anion. The Ag-N bond distance of 2.117 Å is similar to that reported in the complex salt $[Ag(dmpzH)_2]_2Cr_2O_7$ (dmpzH = 3,5-dimethylpyra-zole) [27]. The bulk structure is achieved by a three-dimensional network of intermolecular N-H···F (2.637 and 2.402 Å), C-H···F (2.558 Å) hydrogen bonds (**Figure 5(a)**) and Ag···F (3.145 Å) interactions (**Figure 5(b)**) that interconnect the ionic constituents. Ag···π (3.222 Å) interactions involving the silver center of one $[Ag(N_2H_{10}C_{11})_2]^+$cation and the π-electrons system of the benzene ring of the adjacent cations (**Figure 5(c)**) provide additional stabilization for the crystal packing.

### 3.6. Theoretical Analysis

The optimized structure, the molecular electrostatic potential and the electron

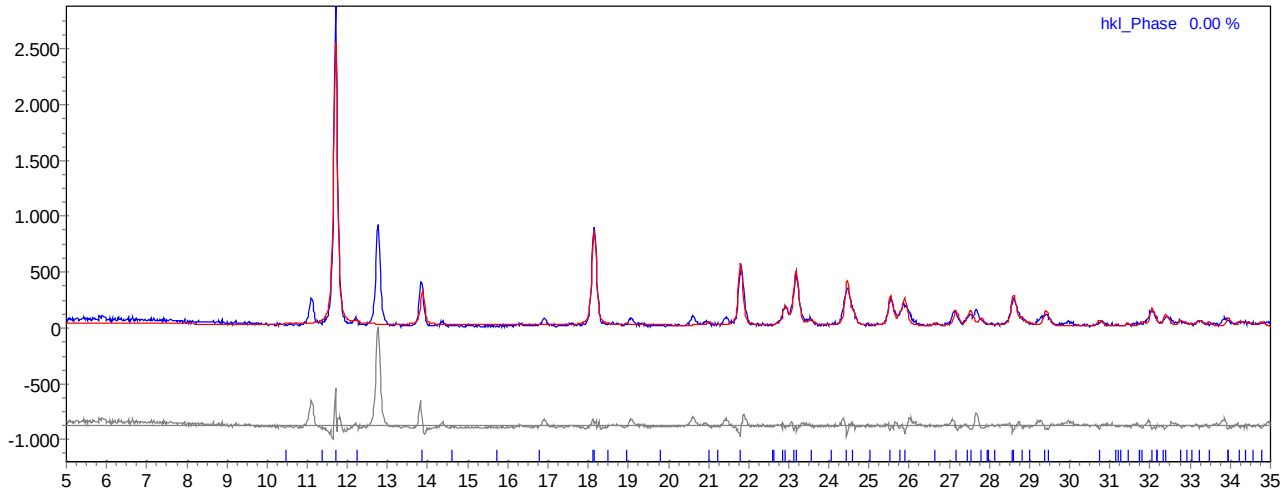


**Figure 2.** Rietveld refinement plot for $[Ag(N_2H_{10}C_{11})_2]PF_6$ with difference plots and peak markers at the bottom. The lowest portions show the high-angle range at a magnified scale (5).

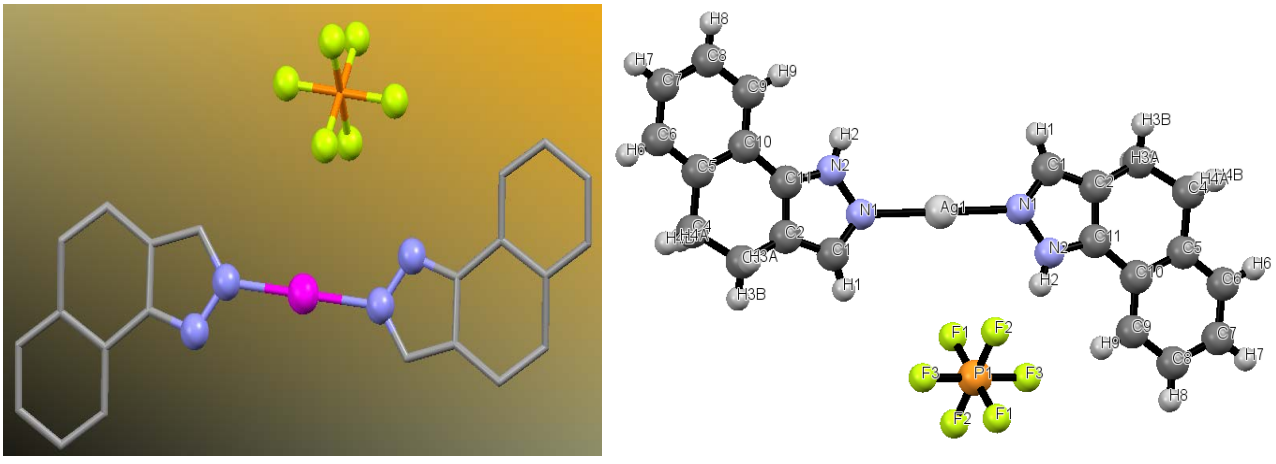


(a) (b)

**Figure 3.** Mercury view (ball and sticks) of the molecular structure of $[Ag(N_2H_{10}C_{11})_2]PF_6$ Ag(pink), N(blue), P(orange), F(greenish yellow) (a); ORTEP view of the molecular structure of $[Ag(N_2H_{10}C_{11})_2]PF_6$ showing the numbering and labeling of the different atoms (b).

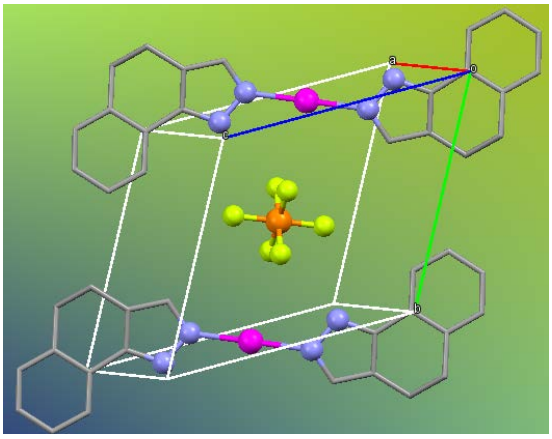


**Figure 4.** Projection of the unit cell of the title compound highlighting the $PF_6^-$ anion sandwiching two centrosymmetric $[Ag(N_2H_{10}C_{11})_2]^+$ cations.

**Table 2.** Summary of Crystallographic data of $[Ag(N_2H_{10}C_{11})_2]PF_6$ obtained from Rietveld refinement on X-ray diffraction pattern.

| Empirical formula | $C_{22}H_{20}AgN_4PF_6$ | |
|---|---|---|
| Formula weight | 593.26 | |
| Temperature | 298 K | |
| Wavelength | 1.5418 Å | |
| Crystal system | Triclinic | |
| Space group | *P*-1 | |
| Unit cell dimensions | a = 7.776 Å | α = 69.27˚. |
| | b = 8.676 Å | β = 89.86˚. |
| | c = 9.226 Å | γ = 74.50˚. |
| Volume | 558.02 Å$^3$ | |
| Z | 1 | |

**Table 3.** Selected bond lengths and angles in the title compound.

| Bonds | Lengths (Å) | Angles | Values (˚) |
|---|---|---|---|
| Ag(1)-N(1) | 2.117 | N(1)-Ag(1)-N(1) | 180.00 |
| N(1)-N(2) | 1.345 | Ag(1)-N(1)-N(2) | 123.45 |
| C(1)-N(1) | 1.322 | C(1)-N(1)-Ag(1) | 129.65 |
| | | C(11)-N(2)-N(1) | 111.39 |
| | | C(2)-C(1)-N(1) | 112.13 |

density map of $[Ag(N_2H_{10}C_{11})_2]PF_6$ are shown in **Figure 6**. The optimized structure (**Figure 6(a)**) shows a complete delocalization of the π-systems of electrons in the pyrazole units and the benzene fractions of the ligands. However, the reproducibility of the optimized geometry is satisfactory even though the symmetry observed around the silver center and the phosphorus atom is lost in the optimized structure. In fact, the corresponding bonds in the two ligand molecules of the optimized structure show a slight discrepancy ranging from 0.000 - 0.008 Å. However, the C3-C4, C5-C6, C6-C7, C10-C11 and the C8-C9 bond lengths remained unaltered in the two ligands. On the average bases, the Ag-N bond length in the optimized structure was elongated to 2.148 Å from 2.117Å in the experimental structure, giving a disparity of 0.031 Å. In the same respect, the N1-N2 bond increased from 1.345 Å to an average of 1.384 Å in the optimized structure, giving a difference of 0.039 Å. This sensitive gap is attributed to the difference between the experimental model (solid phase) and gas phase model. All other corresponding bond lengths experienced slight elongation in the optimized structure, resulting to a general disparity ranging from 0.004 Å to 0.197 Å. These changes in the optimized bond lengths result to corresponding changes in bond angles and dihedral angles. For instance, the linear N1-Ag-N1 angle in the experimental structure was distorted to 173.20˚ in the optimized structure.

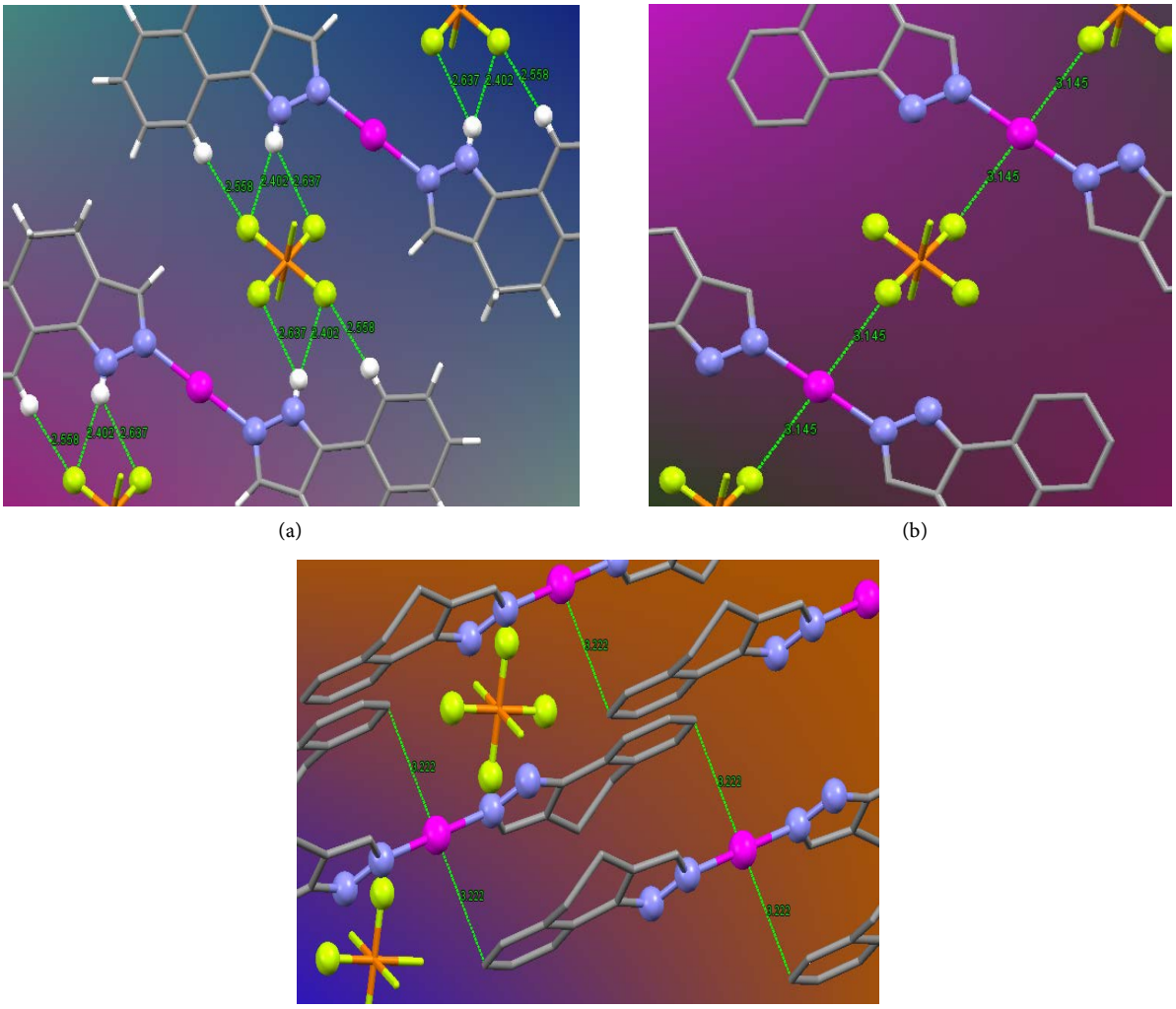


(a) (b)

(c)

**Figure 5.** Intermolecular (a) N-H···F (2.637 and 2.402 Å), C-H···F (2.558 Å); (b) Ag···F (3.145 Å) and (c) Ag···π (3.222 Å) interactions in the title compound.

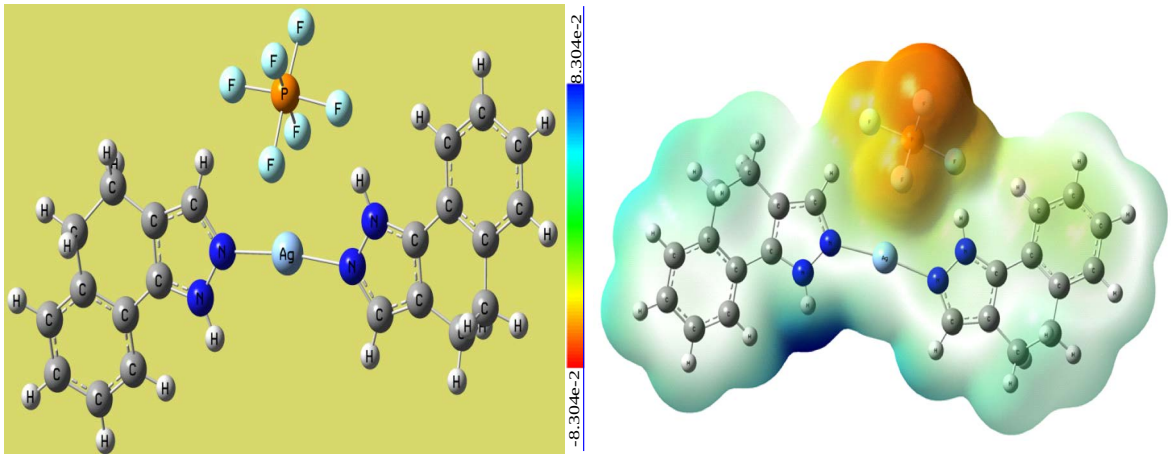


(a) (b)

**Figure 6.** Optimized structure (a) and Molecular electrostatic potential and the electron density map (b) of $[Ag(N_2H_{10}C_{11})_2]PF_6$ at an isosurface value of 0.020 a.u. and an isodensity of 0.0004 a.u.

In order to study the site of $[Ag(N_2H_{10}C_{11})_2]PF_6$ available for electrophilic and nucleophilic attack, the molecular electrostatic potential (MEP) map (**Figure 6(b)**) was plotted. This map also gives an insight on the size, shape and charge density of the title compound. Different values of the electrostatic potential at the surfaces are represented by different colors; red represents regions of most negative electrostatic potential, blue represents regions of most positive electrostatic potential and green represents regions close to zero electrostatic potential. Thus, the most positive region of the MEP map of this complex is localized over the N-H group of the ligand, indicating that they are the most susceptible sites for nucleophilic attack. Meanwhile, the red and orange regions around the fluorine atoms of $PF_6^-$ indicate that the region is rich in electron density and are the most suitable for electrophilic attacks. Some global reactivity descriptors of the complex, were obtained as follows; $I$ = 144.79 kcal/mol, $A$ = 42.48 kcal/mol, $\mu$ = −93.64 kcal/mol, $\eta$ = 51.16 kcal/mol, $S$ = 0.00977 mol/kcal and $\omega$ = 85.70 kcal/mol. The FT-IR vibrational frequencies of $[Ag(N_2H_{10}C_{11})_2]PF_6$ were also obtained using the LanL2DZ basis set. Selected calculated IR vibrational frequencies ($cm^{-1}$) of $[Ag(N_2H_{10}C_{11})_2](PF_6)$ complex and their assignment are presented in **Table 4**. It is worth noting that, the N-H stretching vibration observed between 3705 - 3455 $cm^{-1}$ is shifted to higher frequency with respect to what is obtained experimentally. Since this experimental frequency range is similar to N-H stretching of imidazole ($C_3H_4N_2$) observed by Ramasamy at 3376 $cm^{-1}$ [28], it could be concluded that to some extent, the experimental results are more reliable than the theoretical. This is concretized by the fact that, the C-H group also shows multiple theoretical vibrational modes at very different frequency values. For instance, the C-H group of the pyrazole unit vibrates at 3292 - 3289 $cm^{-1}$, while the benzene fragment of this compound shows symmetric and asymmetric C-H stretching at 3232 - 3231 $cm^{-1}$ and 3211 $cm^{-1}$ respectively. To add, the cyclohexane part of this complex exhibits C-H scissoring at 1353 $cm^{-1}$, rocking at 1396 - 1361 $cm^{-1}$ and twisting in the interval 1517 - 1502 $cm^{-1}$.

**Table 4.** Selected calculated IR vibrational frequencies ($cm^{-1}$) of $[Ag(N_2H_{10}C_{11})_2](PF_6)$ complex and their assignment.

| Vibrational assignment | Calculated frequencies ($cm^{-1}$) | Vibrational assignment | Calculated frequencies ($cm^{-1}$) |
|---|---|---|---|
| $\bar{\upsilon}(N\text{-}H)_{py,\,s}$ | 3455 - 3705 | $\bar{\upsilon}(C\text{-}H)_{cy,sc}$ | 1353 |
| $\bar{\upsilon}(C\text{-}H)_{py,s}$ | 3289 - 3292 | $\bar{\upsilon}(C\text{-}H)_{cy,\,ben,\,sc}$ | 1217 - 1235 |
| $\bar{\upsilon}(C\text{-}H)_{ben,ss}$ | 3231 - 3232 | $\bar{\upsilon}(C\text{-}C)_{cy,\,t}$ | 1039 - 1063 |
| $\bar{\upsilon}(C\text{-}H)_{\,ben,as}$ | 3211 | $\bar{\upsilon}(N\text{-}H,\,C\text{-}H)_{py,\,t}$ | 877 |
| $\bar{\upsilon}(C{=}C,C{=}N)_{py,\,ben,s}$ | 1522 - 1665 | $\bar{\upsilon}(P\text{-}F)_{as}$ | 815 - 825 |
| $\bar{\upsilon}(C\text{-}H)_{cy,\,t}$ | 1502 - 1517 | $\bar{\upsilon}(C\text{-}H)_{ben,\,w}$ | 804 - 809 |
| $\bar{\upsilon}(C\text{-}H)_{py,\,ben,r}$ | 1465 - 1496 | $\bar{\upsilon}(Ag\text{-}N)_r$ | 129 - 136 |
| $\bar{\upsilon}(C\text{-}H)_{cy,r}$ | 1361 - 1396 | | |

$\bar{\upsilon}$, represents vibration; *py,* stands for pyrazole; *s,* indicates stretching; *ben,* represents benzene; *ss* denotes symmetric stretching; *as,* is asymmetric stretching; *cy,* represents cyclohexane; *t,* stands for twisting; *sc*, is scissoring; w indicates wagging and *r* represents rocking.

Meanwhile, the experimental C-H vibration (2953 $cm^{-1}$ and 2832 $cm^{-1}$) is in agreement with literature [29]. Peculiar also of the theoretical IR results is the C=C and C=N stretching in the region 1665 - 1522 $cm^{-1}$ which is quite similar to the interval 1618 - 1543 $cm^{-1}$ obtained experimentally. Finally, the theoretically $PF_6^-$ asymmetric and symmetric stretching, noticed between 825 $cm^{-1}$ and 600 $cm^{-1}$ respectively, is very close to the experimental range and those reported in literature [26].

The DFT elucidation shows that $[Ag(N_2H_{10}C_{11})_2]PF_6$ has 358 molecular orbitals (MO), 129 occupied molecular orbital and 229 unoccupied molecular orbitals. The highest occupied molecular orbital, HOMO, is the 129$^{th}$ MO (**Figure 7(a)**) and has an energy of −144.79 kcal/mol while the lowest unoccupied molecular orbital (LUMO) which is the 130$^{th}$ MO (**Figure 7(b)**) has an energy of −42.48 kcal/mol. The red and green colors represent the positive and negative phases of the molecular orbitals respectively. The $Ag^+$ metal center makes 3.036% contributions to the HOMO and 1.748% to the LUMO. $PF_6^-$ makes negligible contributions to both the HOMO and LUMO. The calculated energy gap of HOMO-LUMO, of value 102.31 kcal/mol explains the ultimate charge transfer interface within the complex and characterizes the chemical reactivity and kinetic stability of the material.

## 4. Conclusion

The Bis(4,5-dihydro-1*H*-benzo[g]indazole)silver(I) hexafluorophosphate salt, $[Ag(N_2H_{10}C_{11})_2]PF_6$, has been synthesized and characterized using various techniques, such as IR and $^1$HNMR spectroscopies, TGA/DTG analyses, Rietveld refinement from powder X-ray diffraction and DFT studies. In the solid, the ionic constituents of the salt are linked through electrostatic and intermolecular interactions. DFT studies in gaseous phase revealed structural preferences of the atoms in $[Ag(N_2H_{10}C_{11})_2]PF_6$, demonstrating disparities between the X-ray and optimized structures in terms of bond lengths and angles, albeit they are within

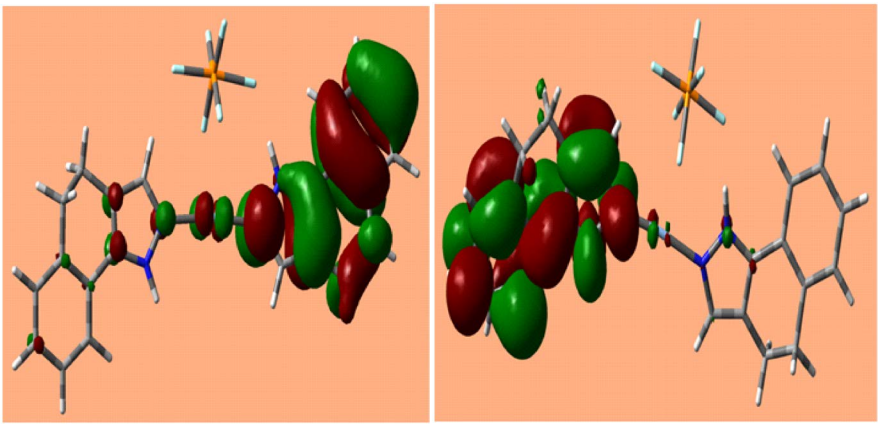

(a) (b)

**Figure 7.** View of highest occupied molecular orbital (a) and lowest unoccupied molecular orbital (b) of $[Ag(N_2H_{10}C_{11})_2]PF_6$.

acceptable ranges. The different IR vibrational frequencies were observed and the approximated reactivity of the material was estimated by the calculation of the ionization energy and the electron affinity of the materials. The $[Ag(N_2H_{10}C_{11})_2]PF_6$ complex salt appears less reactive and more chemically stable than the related $[Ag(N_2C_{11}H_{10})_2]NO_3$ reported earlier [16]. However, just like the case with $[Ag(N_2C_{11}H_{10})_2]NO_3$, the N-H group of the present compound $[Ag(N_2H_{10}C_{11})_2]PF_6$ provides site for nucleophilic attacks while the fluorine atoms of the uncoordinated hexafluorophosphate are susceptible for electrophilic attacks.

## Acknowledgements

The authors are grateful to Prof Norberto Masciocchi of the Università del l'Insubria (Como, Italy) for X-ray facilities and to Prof C. Pettinari of the University of Camerino (Camerino, Italy) for spectroscopic analysis facilities.

## References

[1] Menozzi, G., Mosti, L., Schenone, P., D'Amico, M., Falciani, M. and Filippelli, W. (1994) 1-Aryl-1H-Pyrazole-5-Acetic Acids with Anti-Inflammatory, Analgesic and Other Activities. *Farmaco*, **49**, 115-119.

[2] Soliman, R., Habib, N.S., Ashour, F.A. and El-Taiebi, M. (2001) Synthesis and Antimicrobial Activity of Novel Pyrazole, Pyrazoline, Pyrazolinone and Pyrazolidinedione Derivatives of Benzimidazole. *Bollettino Chimico Farmaceutico*, **140**, 140-148.

[3] Liu, X.H., Cui, P., Song, B.A., Bhadury, P.S., Zhu, H.L. and Wang, S.F. (2008) Synthesis, Structure and Antibacterial Activity of Novel 1-(5-substituted-3-substituted-4,5-dihydropyrazol-1-yl)ethanone Oxime Ester Derivatives. *Bioorganic & Medicinal Chemistry*, **16**, 4075-4082. https://doi.org/10.1016/j.bmc.2008.01.035

[4] Trofimenko, S. (1972) The Coordination Chemistry of Pyrazole-Derived Ligands *Chemical Reviews*, **72**, 497-509.

[5] Ten-Hoedt, R.W., Driessen, W.L. and Verschoor, G. (1983) Structure of Hexakis(pyrazole)nickel(II) Bis(tetrafluoroborate), $[Ni(C_3H_4N_2)_6](BF_4)_2$. *Acta Crystallographica*, **C39**, 71-72.

[6] Reimann, C.W., Santoro, A. and Mighell, A.D. (1970) The Crystal and Molecular Structure of Hexapyrazolenickel(II) Nitrate, $Ni(C_3H_4N_2)_6(NO_3)_2$. *Acta Crystallographica*, **B26**, 521-526. https://doi.org/10.1107/S0567740870002741

[7] Lumme, P.O., Lindell, E. and Mutikainen, I. (1988) *Trans*-Hexakis(pyrazole)manganese(II) Bisperchlorate (1) and *Trans*-Dichlorotetrakis(pyrazole)manganese(II) (2). *Acta Crystallographica*, **C44**, 967-970. https://doi.org/10.1107/S0108270188001131

[8] Pettinari, C., Marinelli, A., Marchetti, F., Ngoune, J., Gallindo, A., Alvarez, E. and Gomez, M. (2010) Sythesis and Coordination Chemistry of Two N2-Donor Chelating Di(indazolyl)methane Ligands: Structural Characterization and Comparison of their Metal Chelating Aptitudes. *Inorganic Chemistry*, **49**, 10543-10556. https://doi.org/10.1021/ic101577k

[9] Ding, L., Grehn, L., De Clercq, E., Andrei, G., Snoeck, R., Balzarini, J., Fransson, B. and Ragnarsson, U. (1994) Synthesis and Antiviral Activity of Three Pyrazole Analogues of Distamycin A. *Acta Chemica Scandinavica*, **48**, 498-505. https://doi.org/10.3891/acta.chem.scand.48-0498

[10] Goslar, J., Sczaniecki, P.B., Strawiak, M.M. and Mrozinski, J. (1988) Chemical-Properties, Magnetic and Epr Studies of Pyrazole Copper(II) Complexes. *Transition Metal Chemistry*, **13**, 81-86. https://doi.org/10.1007/BF01087793

[11] Ovejero, P., Mayoral, M.J., Cano, M. and Lagunas, M.C. (2007) Luminescence of Neutral and Ionic Gold(I) Complexes Containing Pyrazole or Pyrazolate-Type Ligands. *Journal of Organometallic Chemistry*, **692**, 1690-1697.

[12] Sakai, K., Tomista, Y., Ue, T., Goshima, K., Ohminato, M., Tsubomura, T., Matsumoto, K., Ohmura, K. and Kawakami, K. (2000) Syntheses, Antitumor Activity, and Molecular Mechanics Studies of *Cis*-$PtCl_2(pzH)_2$ (pzH = pyrazole) and Related Complexes. Crystal Structure of a Novel Magnus-Type Double-Salt $[Pt(pzH)_4][PtCl_4][cis\text{-}PtCl_2(pzH)_2]_2$ Involving Two Perpendicularly Aligned 1D Chains. *Inorganica Chimica Acta*, **297**, 64-71.

[13] Kratz, F., Nuber, B., Weiss, J. and Keppler, B.K. (1992) Synthesis and Characterization of Potential Antitumour and Antiviral Gallium(III) Complexes of N-Heterocycles. *Polyhedron*, **11**, 487-498.

[14] Schore, N.E. (2007) Study Guide and Solutions Manual for Organic Chemistry: Structure and Function. 5th Edition, W.H. Freeman and Company, New York.

[15] Rheingold, A.L., Ostrander, R.L., Haggerty, B.S. and Trofimenko, S. (1994) Homoscorpionate (Tris(pyrazolyl)borate) Ligands Containing Tethered 3-phenyl Groups. *Inorganic Chemistry*, **33**, 3666-3676. https://doi.org/10.1021/ic00095a009

[16] Fomuta, T.R., Djimassingar, G., Ngoune, J., Ngnabeuye, N.O., Anguile, J.J. and Nenwa, J. (2017) Synthesis, Structural Characterization and DFT Studies of Silver(I) Complex Salt of Bis(4,5-dihydro-1*H*-benzo[g]indazole). *Crystal Structure Theory and Applications*, **6**, 11-24. https://doi.org/10.4236/csta.2017.62002

[17] TOPAS-R (2005) V.3.0, Bruker AXS, Karlsruhe, Germany.

[18] March, A.Z. (1932) Mathematische Theorie der Regelung nach der Korngestah bei Affiner Deformation. *Kristallographie*, **81**, 285-297. https://doi.org/10.1524/zkri.1932.81.1.285

[19] Dollase, W.A. (1986) Correction of Intensities for Preferred Orientation in Powder Diffractometry: Application of the March Model. *Journal* of *Applied Crystallography*, **19**, 267-272. https://doi.org/10.1107/S0021889886089458

[20] Amsterdam Density Functional (ADF) Version 2007.01. http://www.scm.com

[21] Umadevi, P. and Lalitha, P. (2012) Synthesis and Antimicrobial Evaluation of Imino Substituted 1, 3, 4 Oxa and Thiadiazoles. *International Journal of Pharmacy and Pharmaceutical Sciences*, **4**, 523-527.

[22] Mebi, A.C. (2011) DFT Study on Structure, Electronic Properties, and Reactivity of Cis-Isomers of $[(NC_5H_4\text{-}S)_2Fe(CO)_2]$. *Journal of Chemical Sciences*, **123**, 727-731. https://doi.org/10.1007/s12039-011-0131-2

[23] Nazmul, I. and Dulal, C.G. (2012) On the Electrophilic Character of Molecules through Its Relation with Electronegativity and Chemical Hardness. *International Journal of Molecular Sciences*, **13**, 2160-2175. https://doi.org/10.3390/ijms13022160

[24] Sayed, I., Kosy, S.M., Abdel, M.F., Hamed, M.A., Gokha, A.A. and Sattar, M.M.A. (2011) One-Pot Synthesis of Novel $\alpha$-Aminophosphonate Derivatives Containing a Pyrazole Moiety. *Journal of American Science*, **7**, 604-608.

[25] Swarnkar, D., Ameta, R. and Vyas, R. (2014) Microwave Assisted Synthesis of Some Pyrazole Derivatives and Their Antibacterial and Antifungal Activity. *The Pharma Innovation Journal*, **3**, 5-9.

[26] Calhorda, M., Costa, P.J., Crespo, M.O., Gimeno, C., Jones, P.G., Laguna, A., Na-

ranjo, M., Quintal, S., Shia, Y. and Villacampa, M.D. (2006) Group 11 Complexes with the Bis(3,5-dimethylpyrazol-1-yl)methane Ligand. How Secondary Bonds can Influence the Coordination Environment of Ag(I): The Role of Coordinated Water in $[Ag_2(\mu\text{-}L)_2(OH_2)_2](OTf)_2$. *Dalton Transactions*, **34**, 4104-4113. https://doi.org/10.1039/B605034D

[27] Beheshti, A., Zafarian, H.R., Khorramdin, R., Monavvar, M.F. and Carmel, T.A. (2012) Novel Silver(I) Pyrazole-Based Coordination Polymers: Synthetic and Structural Studies. *Polyhedron*, **48**, 245-252.

[28] Ramasamy, R. (2015) Vibrational Spectroscopic Studies of Imidazole. *Armenian Journal of Physics*, **8**, 51-55.

[29] Yongxiu, L. and Zhaoai, N. (1993) The Coordination between Silver Nitrate and Open Chain Polyether. *Transactions of Nonferrous Metals Society of China*, **3**, 38-41.